



# RESEARCH MEMORANDUM

EXPERIMENTAL INVESTIGATION OF A TWO-DIMENSIONAL SPLIT-WING

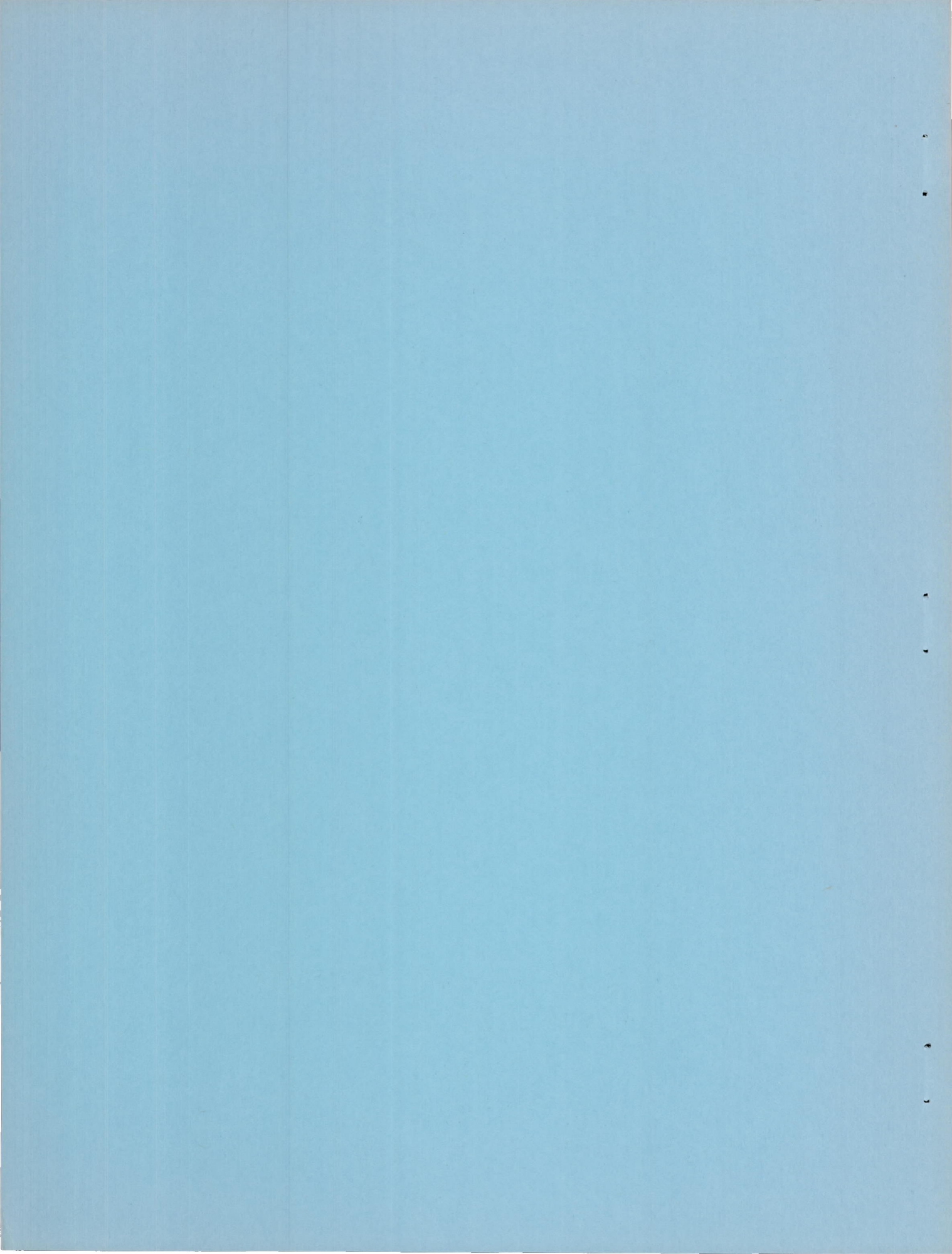
RAM-JET INLET AT MACH NUMBER OF 3.85

By James F. Connors and Richard R. Woollett

Lewis Flight Propulsion Laboratory  
Cleveland, Ohio

NATIONAL ADVISORY COMMITTEE  
FOR AERONAUTICS  
WASHINGTON

August 11, 1952  
Declassified June 20, 1957



## NATIONAL ADVISORY COMMITTEE FOR AERONAUTICS

RESEARCH MEMORANDUM

## EXPERIMENTAL INVESTIGATION OF A TWO-DIMENSIONAL SPLIT-WING

## RAM-JET INLET AT MACH NUMBER OF 3.85

By James F. Connors and Richard R. Woollett

## SUMMARY

An experimental investigation of the performance characteristics of a two-dimensional isentropic diffuser, suitable for split-wing ram-jet application, has been conducted at a Mach number of 3.85 in the Lewis 2- by 2-foot supersonic tunnel. The inlet, which had a 4-inch maximum depth and a 10-inch span, was mounted on a typical wing section equipped with a variable exit and a force-measuring system. Pressure-recovery and mass-flow data are presented for a range of angle of attack from  $0^\circ$  to  $4^\circ$ . Aerodynamic force data at zero angle of attack are also included.

A maximum total-pressure recovery of 0.41, corresponding to a kinetic energy efficiency of 90 percent, was obtained at zero angle of attack with a maximum mass-flow ratio of 0.95. As the angle of attack was increased to  $4^\circ$ , the pressure recovery decreased to 0.34 and the maximum mass-flow ratio decreased to 0.91. In every case, a large discontinuity in both pressure recovery and mass flow with a characteristic hysteresis was encountered between supercritical and subcritical operation as a consequence of the twin-duct arrangement of the diffuser. Schlieren observations indicated an asymmetrical subcritical shock pattern with large-scale separation and spillage occurring on one passage only. Large changes in all the aerodynamic force coefficients caused by such asymmetrical flow make subcritical operation intolerable for any flight application.

## INTRODUCTION

Theoretical analyses of the ducted-airfoil ram jet (references 1 and 2) have indicated that this type of power-plant configuration has considerable promise for application on long-range or interceptor-type aircraft operating at Mach numbers of 2 or above. In addition,

the study by Consolidated Vultee Aircraft Corporation has indicated that there are no structural limitations that prevent operation at the higher Mach numbers and altitudes. This latter conclusion is largely the result of the development of the can-type combustor with its provisions for the cooling of external skin surfaces.

A need, therefore, exists for substantiation of the diffuser performance assumed in such analyses. The purpose of the present study, then, is (1) to experimentally evaluate the performance of a two-dimensional diffuser designed for efficient operation at a Mach number of 3.85 and suitable for ducted-airfoil ram-jet application and (2) to measure the aerodynamic forces on an experimental wing engine installation. Accordingly, an inlet designed for both external and internal isentropic compression was mounted on a typical wing section and was studied over a range of angle of attack from  $0^\circ$  to  $4^\circ$ .

#### SYMBOLS

The following symbols are used in this report:

$A_i$	inlet capture area, sq ft
$A_{\max}$	maximum frontal area of engine, sq ft
$A_w$	wing plan area (chord measured from leading edge of cowl lip to base), sq ft
$A_4$	nozzle-exit area, sq ft
$C_D$	external drag coefficient ( $D/q_0 A_{\max}$ )
$C_L$	lift coefficient ( $L/q_0 A_{\max}$ )
$C_M$	pitching-moment coefficient ( $Nl/q_0 A_{\max}^c$ )
$C_N$	normal-force coefficient ( $N/q_0 A_w$ )
$C_P$	propulsive-thrust coefficient ( $F-D/q_0 A_{\max}$ )
$c$	over-all distance measured from leading edge of wedge to the base, ft
$D$	external drag, lb
$F$	thrust, lb

L	lift, lb
l	moment arm from leading edge of wedge, ft
M <sub>0</sub>	free-stream Mach number
m <sub>e</sub>	mass-flow rate through engine, slugs/sec
m <sub>0</sub>	mass-flow rate through a free-stream tube area equal to A <sub>i</sub> , slugs/sec
N	normal force, lb
P <sub>0</sub>	free-stream total pressure, lb/sq ft
P <sub>3</sub>	diffuser-exit total pressure, lb/sq ft
p <sub>0</sub>	free-stream static pressure, lb/sq ft
q <sub>0</sub>	free-stream dynamic pressure ( $\gamma p_0 M_0^2 / 2$ ), lb/sq ft
$\alpha$	angle of attack, deg
$\gamma$	ratio of specific heats
$\mu^2 \tau$	simulated combustion parameter where $\mu$ equals one plus the fuel-air ratio and $\tau$ equals the total-temperature ratio across the combustion chamber

#### APPARATUS AND PROCEDURE

The experimental investigation was conducted in the NACA Lewis 2- by 2-foot supersonic tunnel at a Mach number of 3.85 and at a simulated pressure altitude of 108,000 feet. The tunnel air was maintained at a temperature of  $200^\circ \pm 5^\circ$  F and at a dew-point temperature of  $-15^\circ \pm 10^\circ$  F. Based on the maximum depth of the wing (4 in.), the Reynolds number was 343,000.

As illustrated in the perspective drawing (fig. 1(a)), the complete model spanned the tunnel and consisted of three separate units - the center section, which was of test interest, and the two side or supporting sections through which the low-energy air in the tunnel boundary layer was bypassed. The center section was positioned between the side sections by six links of a three-component balance system (see fig. 1(b) for linkage details). A large yoke was used to connect the trunnions on the side sections and thus permit changes in the angle of attack of the model. Mounted downstream and independent of the

model, a variable-exit plug was employed to regulate the inlet back pressure. Important over-all dimensions of the model are given in the schematic drawing of figure 1(c). Pressure instrumentation (fig. 1(d)) consisted of total- and static-pressure rakes mounted at the diffuser exit and immediately upstream of the variable outlet. In addition, static-pressure taps were located on the base of the model for evaluation of the base pressure tare loads.

The supersonic diffuser initially investigated was designed for both external and internal isentropic compression. The external compression waves were focused at the lip of the cowl and reduced the flow Mach number to 2.38 at the entrance, while the internal compression waves intersected the centerbody surface in a distributed manner and further reduced the Mach number to 1.40 at the throat. The required external and internal contours were conveniently derived by utilizing the reverse of two Prandtl-Meyer expansions in series. A correction for the displacement thickness of a fully turbulent boundary layer was made to the centerbody contour by using the method of reference 3 even though the pressure gradients experienced were in excess of those for which the theory might be expected to apply. It was assumed that an initially turbulent boundary layer could be assured by the use of artificial roughness on the leading edge of the centerbody.

To overcome the starting problem encountered with high internal-contraction ratios, the inlet was designed for variable geometry by providing for a longitudinal movement of the center wedge. This translation was produced by a small electric motor and screw arrangement installed inside the centerbody. To eliminate edge effects and to maintain a two-dimensional flow into the inlet, and also to permit schlieren flow observations, glass plates were mounted at the sides of the compression wedge.

The subsonic portion of the diffuser was designed for an average angle of divergence between the cowl and the centerbody walls of  $10^{\circ}$ , which was in accord with the data presented in reference 4. However, this subsonic passage was further modified to accommodate a very small diffusion rate near the throat for increased shock stability; a maximum divergence angle of  $14^{\circ}$  existed at the exit of this subsonic diffuser.

From results of experiments with the variable-geometry inlet, an optimum internal contraction was determined and a fixed-geometry diffuser was fabricated. The contours of the variable inlet were modified for the fixed-geometry configuration in order to increase the capture mass flow and decrease the cowl pressure drag. Coordinates of the original and modified inlet are given in figure 1(e).

Cold-flow experiments were conducted wherein the simulation of heat addition was effected by means of a variable-outlet restriction.

The exit plug was mounted independent of the model to allow the balance system to measure forces that were the same as that of a ram jet with burning and choking in a constant-area duct. Tare forces acting on the base, the glass side plates, and the instrumentation lines were evaluated and the appropriate corrections made. Complete pressure data were taken over a range of exit plug positions at angles of attack of  $0^\circ$ ,  $1^\circ$ ,  $2^\circ$ ,  $3^\circ$ , and  $4^\circ$ .

## RESULTS AND DISCUSSION

One of the most difficult problems that arises in the design of high Mach number inlets is that of predicting the effects and the nature of the boundary layer along the compression surface with its strong adverse pressure gradients. Some interesting schlieren photographs of the air flow along the contoured center wedge are presented in figure 2. With a smooth leading edge (fig. 2(a)), there was a characteristic thickening and thinning of the observed boundary layer as it developed along the compression surface. This flow pattern is interpreted as a separation of the laminar boundary layer, followed by reattachment. Transition to a turbulent layer is believed to have occurred by the time the flow entered the diffuser. With the large adverse pressure gradients encountered here, separation of the laminar boundary layer would be expected theoretically, as indicated by the prediction of a laminar separation point by the method of reference 5 (see arrow on fig. 2(a)). On further inspection of the schlieren photograph, it is observed that there are discontinuous lines or striations within the apparent boundary-layer region. The reason for this is not known. Subsequent experiments showed that the addition of leading-edge roughness (a  $1/8$ -inch band of number 100 Carborundum grit) would alter the flow pattern along the compression surface to that shown in the schlieren photograph of figure 2(b). The action of the roughness is presumably to force transition to a turbulent layer which is more stable and resistant to flow separation. As noted in figure 2(b), the observed boundary layer followed the contour of the wedge more closely and indicated no flow separation. However, the over-all pressure recovery of the inlet was somewhat lower (2 or 3 percent) with the use of leading-edge roughness. Consequently, no further consideration was given to the use of artificial transition, and the data will be presented only for the inlet with a smooth leading edge.

### Original Isentropic Inlet (with Variable Geometry)

The original inlet design incorporated a large amount of internal compression with provisions for a variable internal-contraction ratio to satisfy the starting requirements. The optimum diffuser performance obtained with this configuration at zero angle of attack was a maximum

total-pressure recovery  $P_3/P_0$  of 0.41 and a corresponding supercritical mass-flow ratio  $m_e/m_0$  of 0.75. These results were obtained with an internal-contraction ratio that approximated the Kantrowitz-Donaldson limiting value (reference 6) corresponding to the design inlet Mach number of 2.38. Larger internal-contraction ratios could not be imposed on the flow without expulsion of the normal shock because of pressure feedback and separation of the boundary layer in the convergent passage.

Schlieren photographs of the flow patterns obtained with this inlet at optimum tip projection and at zero angle of attack are presented in figure 3 for both supercritical and subcritical operating conditions. As may be observed in the photograph of the supercritical flow pattern (fig. 3(a)), the compression shocks emanating from the contoured centerbody coalesced well ahead of the cowl lip with a resultant large amount of flow spillage. This resulted from the fact that the inlet was designed for optimum performance with a more fully retracted centerbody, that is, with more internal contraction.

As the flow became subcritical, there occurred a large discontinuity in both pressure recovery and mass-flow ratio. Concomitantly, an asymmetrical shock pattern was observed at the inlet (see fig. 3(b)). In the bottom passage, the flow had completely separated up to the leading edge of the wedge with subsonic or possibly reverse flow in the inlet while in the top passage the flow maintained its supercritical shock pattern. This phenomenon will be discussed more fully in connection with the final modified inlet.

The possibility of obtaining additional internal compression and correspondingly higher pressure recoveries by means of variable geometry appeared to depend on the development of a boundary-layer control system that could adequately cope with the feedback problem. In the present study, tunnel limitations, associated with the large size of the model, prevented incorporation of a bleed system involving flow spillage into the side passages.

#### Modified Isentropic Inlet (with Fixed Geometry)

In order to arrive at a more practical aerodynamic configuration, some modifications were made to the original inlet. The inlet lip height was increased to capture a larger free-stream tube of air and also to reduce the cowl pressure drag by reducing the projected frontal area. Schlieren photographs of the shock pattern (fig. 3(a)) were then scaled to establish the focal point of the compression waves emanating from the wedge surface, thus locating the desired lip position for the

modified cowl. The internal flow passages were also reworked to impose the Kantrowitz contraction ratio on the flow as indicated from the variable geometry data.

The performance of this configuration at zero angle of attack is presented in figure 4. A maximum total-pressure recovery of 0.41, corresponding to a kinetic energy efficiency of 90 percent at Mach number 3.85, was obtained with a supercritical mass-flow ratio of 0.95. The corresponding schlieren photograph of the inlet flow during supercritical operation (fig. 4(a)) indicated very little flow spillage, and the oblique shock wave from the leading edge appeared to intercept the cowl lip very closely. Unfortunately, a small scratch in the glass occurred immediately ahead of the top cowl lip and care must be exercised in locating the leading edge. As illustrated by the data (fig. 4(a)), there was again a large discontinuity in both mass flow and pressure recovery between critical and subcritical operation. This large detrimental change in engine operating conditions was not of the magnitude ordinarily experienced with internal contraction diffusers; it was accompanied by a pronounced hysteresis loop and by an asymmetric subcritical shock pattern as shown in the schlieren photograph (fig. 4(b)). At zero angle of attack this asymmetric separation pattern would establish itself in either the top or bottom passage with an apparent random selection. This effect was a consequence of the twin-duct arrangement of the diffuser. The hysteresis loop in the curves is explained by the fact that there is a range of outlet-area conditions for which flow continuity can be satisfied by either of two flow patterns at the inlet, (1) supercritical operation with high pressure recovery and a high mass flow through the exit or (2) low pressure recovery and a low mass flow through the exit, which is made possible, in a multiduct system, by one passage undergoing flow reversal and actually spilling flow out of the front of the model. That some of the flow actually circulated around the centerbody (entering the top passage and discharging from the bottom passage) is indicated by the observation that the subcritical mass-flow ratios were less than half of the supercritical value and that the top passage maintained the same flow pattern (and thus had the same mass flow entering) during both supercritical and subcritical engine operation. During subcritical operation it was observed that the angle of the wedge formed by the separated flow varied with the engine exit area in order to spill more or less mass flow as required by continuity considerations. The elimination of this twin-duct interaction may possibly be accomplished by equalizing the pressures in the top and bottom passages by means of interconnecting channels (reference 7).

In figures 5 to 8, the performance curves for this modified isentropic inlet are presented for angles of attack of  $1^\circ$ ,  $2^\circ$ ,  $3^\circ$ , and  $4^\circ$ . In general, the trends were quite similar to that obtained at zero

angle of attack. At each angle of attack, there again was the characteristic hysteresis loop and subcritical asymmetrical shock pattern. As the angle of attack of the model was increased, the critical value of outlet-inlet area ratio increased and thus indicated a reduced back pressure on the diffuser. Therefore, for each supercritical exit condition there is a limiting angle of attack below which the asymmetric inlet flow pattern and the attendant hysteresis is avoided. Thus, if it were specified for this engine operating with fixed geometry and constant heat addition (and thereby constant inlet back pressure) that there can be no subcritical operation at a maximum angle of attack of  $4^\circ$ , the performance at zero angle of attack would then be limited to a maximum recovery of 0.35.

The effect of angle of attack on maximum total-pressure recovery and supercritical mass-flow ratio is shown in the summary curves of figure 9. As the angle of attack was increased from  $0^\circ$  to  $4^\circ$ , the maximum pressure recovery decreased from 0.41 to 0.34 and the supercritical mass-flow ratio decreased from 0.95 to 0.91.

At positive angles of attack, the flow consistently separated subcritically and spilled from the top passage. It was also noted that, as the inlet was moved through the angle-of-attack range from  $0^\circ$  to  $4^\circ$ , the extent of the laminar boundary-layer separation off the top compression surface increased quite markedly (compare figs. 4(b) and 8(b)).

Some total-pressure profiles (indicative of the velocity distributions) across the diffuser exit are presented in figure 10 for the conditions of maximum recovery at each angle of attack and for a typical subcritical point at zero angle of attack. In each case, the flow was found to separate from the centerbody walls. This was probably a consequence of the subsonic diffuser design in which a short length with a resulting high diffusion rate was specified. As expected, the difference in profiles between the top and bottom passages increased with angle of attack. The profiles for subcritical operation (fig. 10(b)) again indicate the possibility of flow reversal in the bottom passage. With flow reversal the pitot pressure probes would have to be rotated  $180^\circ$  to measure the true total pressure.

#### Aerodynamic Force Coefficients at Zero Angle of Attack

Unfortunately a breakdown of the balance system prevented the complete range of force data from being obtained and limits the discussion to zero angle-of-attack data and to the slope of the normal force curve obtained from limited data. The force coefficients are presented in figure 11 as a function of the simulated combustion parameter  $\mu^2 \tau$ , which is indicative of the amount of heat release that would be required in the flight model with burning and choking in a constant-area duct.

As such, the magnitudes of  $\mu^2\tau$  are beyond the range of present-day hydrocarbon fuels. Of course, in the practical flight configuration convergent-divergent exhaust nozzles would be employed so that much smaller values of  $\mu^2\tau$  would be demanded of the combustor and correspondingly smaller values of available thrust would be realized.

These force data serve primarily to illustrate the intolerable operating conditions obtained as the inlet flow pattern became asymmetric. As a value of the simulated combustion parameter  $\mu^2\tau$  of approximately 7.1 was slightly exceeded, the maximum propulsive thrust coefficient  $C_P$  of 1.40 decreased to zero and the external drag coefficient  $C_D$  was doubled from 0.3 to 0.6 as the engine operation became subcritical. The absolute magnitude of the supercritical  $C_D$  of 0.3 was much greater than calculated values showing a maximum of 0.2. This discrepancy may be attributed partly to error in the balance measurements and partly to such tunnel factors as tunnel side-wall interference effects and flow deviations of the air stream relative to the test-section walls which would effectively put the inlet at a slight angle of attack.

Further illustration of the adverse subcritical operating conditions is given in figures 11(c) and 11(d), where the discontinuity is evidenced by a large change in both lift and pitching-moment coefficients. These effects may be illustrated by the following example. If it were assumed that the adverse shift in pitching-moment coefficient ( $\Delta C_M \approx 0.27$ ) were of the same order of magnitude at  $4^\circ$  angle of attack as obtained at zero, the wing would be subjected to an abrupt change in the center of pressure location equal to approximately 9 percent of the chord. Finite values of  $C_L$  and  $C_M$  obtained with supercritical operation presumably result from a slight flow deviation in the tunnel, inasmuch as the model was installed parallel to the tunnel floor for the zero angle-of-attack case.

Sufficient force measurements were taken at a  $2^\circ$  angle of attack to indicate that the slope for the normal force curve was

$$\frac{dC_N}{da} = 0.025/\text{deg}$$

where  $C_N$  is referenced to the wing plan area with a chord measured from the leading edge of the cowl lip to the base. By way of comparison, the two-dimensional Ackeret value for thin wings at small angles of attack is

$$\frac{dC_N}{d\alpha} = \frac{4\pi}{180 \sqrt{M_0^2 - 1}} = 0.019/\text{deg}$$

The contribution of the internal flow to the normal force coefficient at angle of attack is

$$\left( \frac{dC_N}{d\alpha} \right)_{int} = \left( \frac{2\pi}{180} \right) \frac{A_i}{A_w} = 0.003/\text{deg}$$

Thus, the theoretical value for the slope of the normal force curve is

$$\frac{dC_N}{d\alpha} = 0.022/\text{deg}$$

#### SUMMARY OF RESULTS

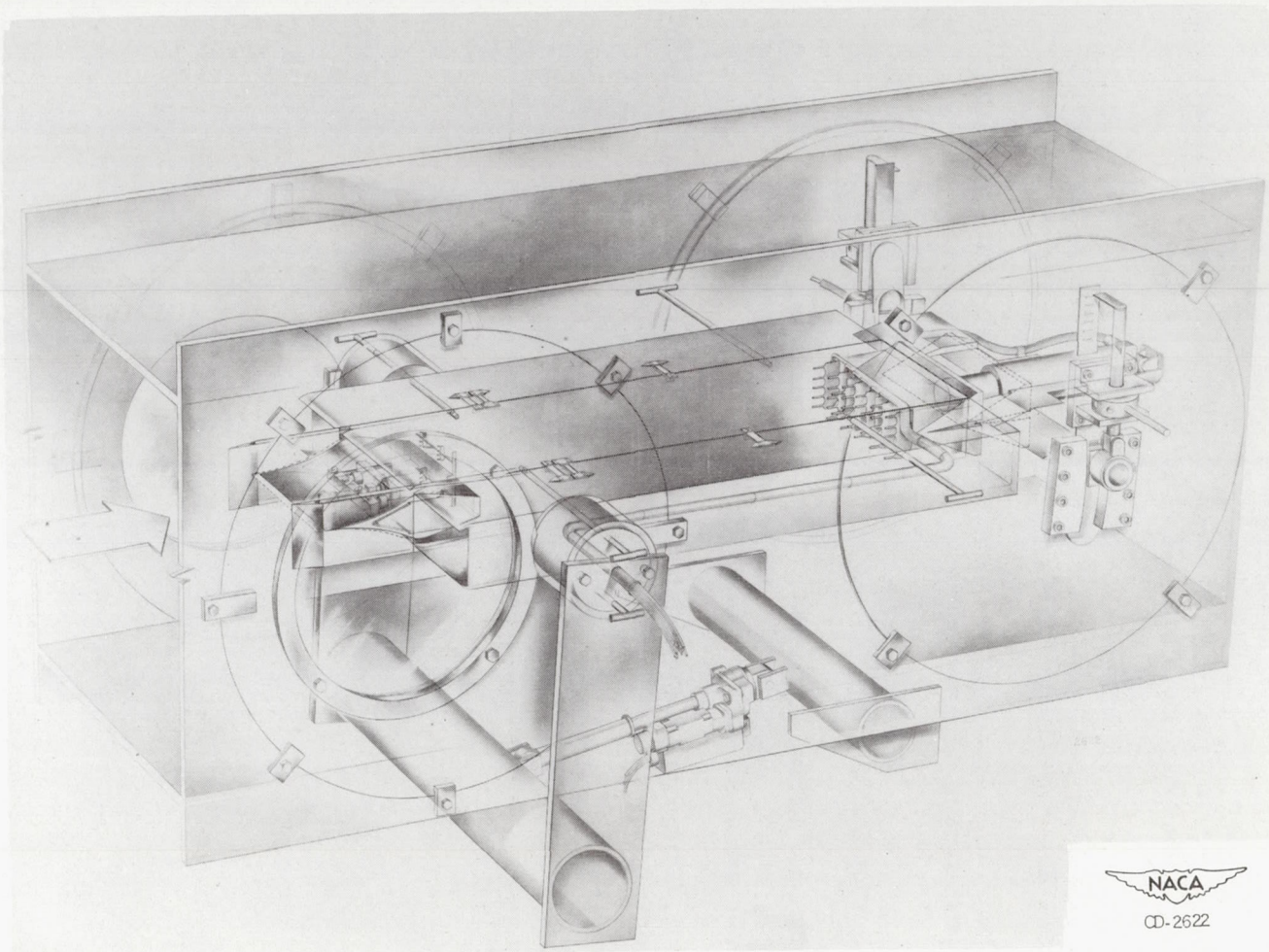
A preliminary experimental investigation of a two-dimensional isentropic inlet suitable for split-wing ram-jet application yielded the following results at a Mach number of 3.85:

1. At zero angle of attack a maximum total-pressure recovery of 0.41, corresponding to a kinetic energy efficiency of 90 percent, was realized with a supercritical mass-flow ratio of 0.95.
2. As the angle of attack was increased to 4°, the maximum total-pressure recovery fell off to 0.34 and the supercritical mass-flow ratio decreased to 0.91.
3. A large discontinuity in both mass flow and pressure recovery with a characteristic hysteresis was encountered between critical and subcritical operation as a consequence of the twin-duct arrangement of the diffuser. Corresponding schlieren photographs showed an asymmetrical subcritical shock pattern with flow spillage occurring out of only one of the passages.
4. The use of variable geometry did not result in the attainment of internal contraction ratios any greater than the Kantrowitz limiting value because of pressure feedback and possible separation of the boundary layer.
5. With a value of the simulated combustion parameter equal to 7.1, a maximum propulsive thrust coefficient of 1.4, based on the maximum frontal area of the engine, was obtained at zero angle of attack. Large changes in all the aerodynamic force coefficients caused by twin-duct interaction made subcritical operation intolerable.

Lewis Flight Propulsion Laboratory  
National Advisory Committee for Aeronautics  
Cleveland, Ohio

REFERENCES

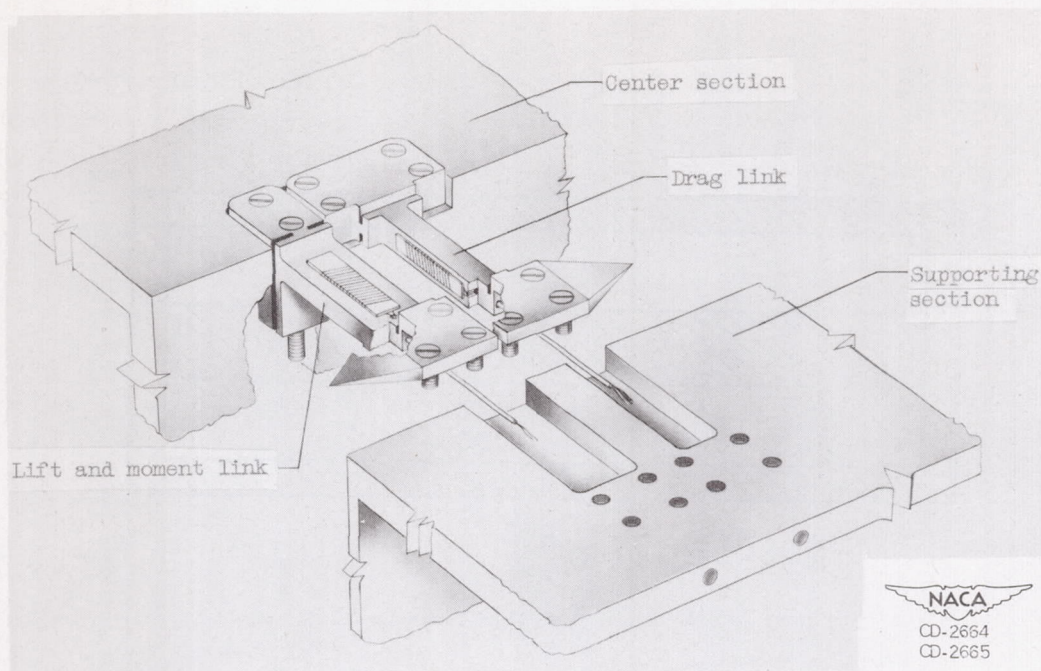
1. Hill, Paul R., and Gammal, A. A.: An Analysis of Ducted-Airfoil Ram Jets for Supersonic Aircraft. NACA RM L7124, 1948.
2. Anon.: Evaluation of Supersonic Split Wing Ram Jets. Convair Rep. No. ZM-9136-001, Consolidated Vultee Aircraft Corp., May, 1949. (Contract No. W35-038ac 17145).
3. Tucker, Maurice: Approximate Calculation of Turbulent Boundary-Layer Development in Compressible Flow. NACA TN 2337, 1951.
4. Patterson, G. N.: Modern Diffuser Design. Aircraft Eng. vol. X, no. 115, Sept. 1938, pp. 267-273.
5. Low, George M.: Simplified Method for Calculation of Compressible Laminar Boundary Layer with Arbitrary Free-Stream Pressure Gradient. NACA TN 2531, 1951.
6. Kantrowitz, Arthur, and Donaldson, Coleman duP.: Preliminary Investigation of Supersonic Diffusers. NACA ACR L5D20, 1945.
7. Leissler, L. A., and Hearth, D. P.: Preliminary Investigation of Effect of Angle of Attack on Pressure Recovery and Stability Characteristics for a Vertical Wedge Nose Inlet at  $M_0 = 1.90$ . NACA RM E52E14, 1952.



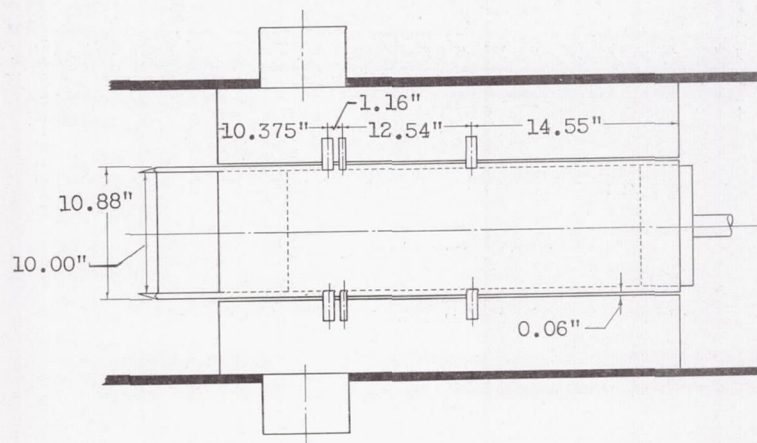
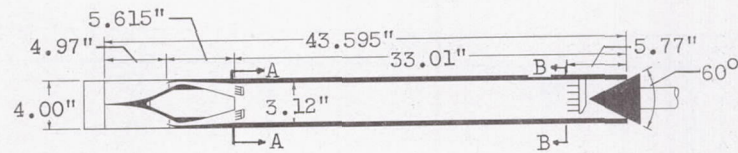
NACA  
CD-2622

(a) Perspective view of split-wing model mounted in NACA Lewis 2- by 2-foot supersonic tunnel.

Figure 1. - Experimental model.



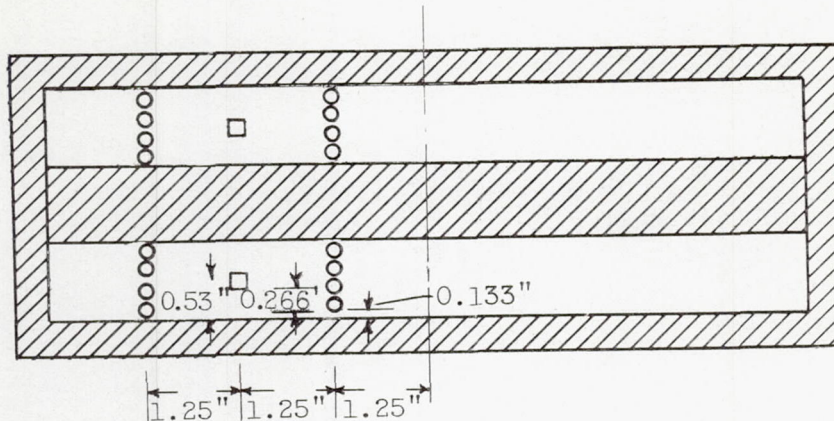
(b) Detail of balance linkages.



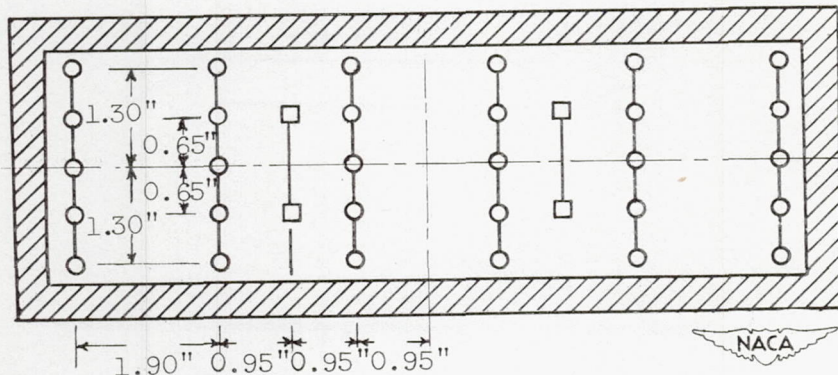
(c) Schematic sketch of model showing important dimensions.

Figure 1. - Continued. Experimental model.

○ Pitot tube  
□ Static tube



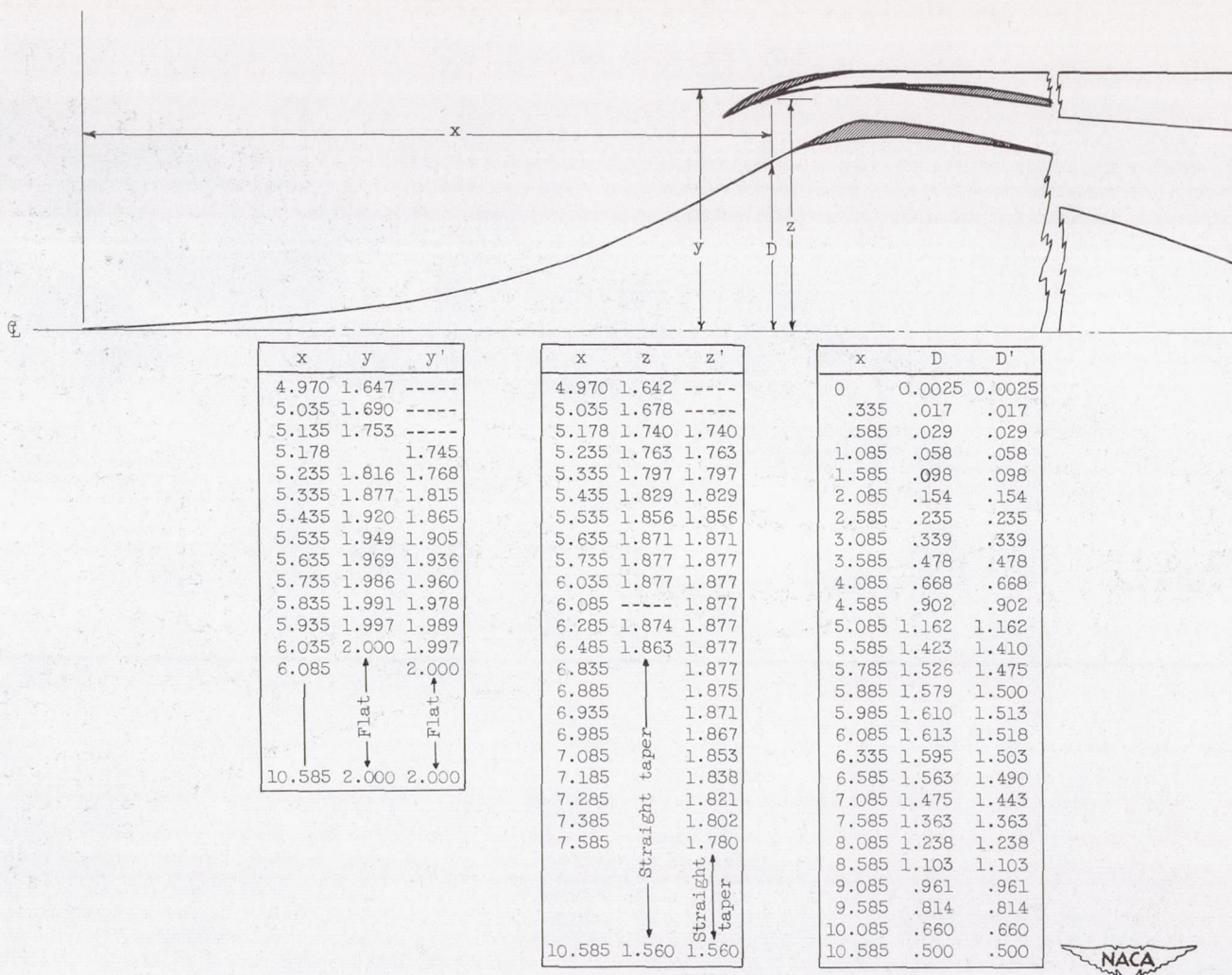
Diffuser-exit rake (section A-A, fig. 1(c))



Combustion-chamber-exit rake (section B-B, fig. 1(c))

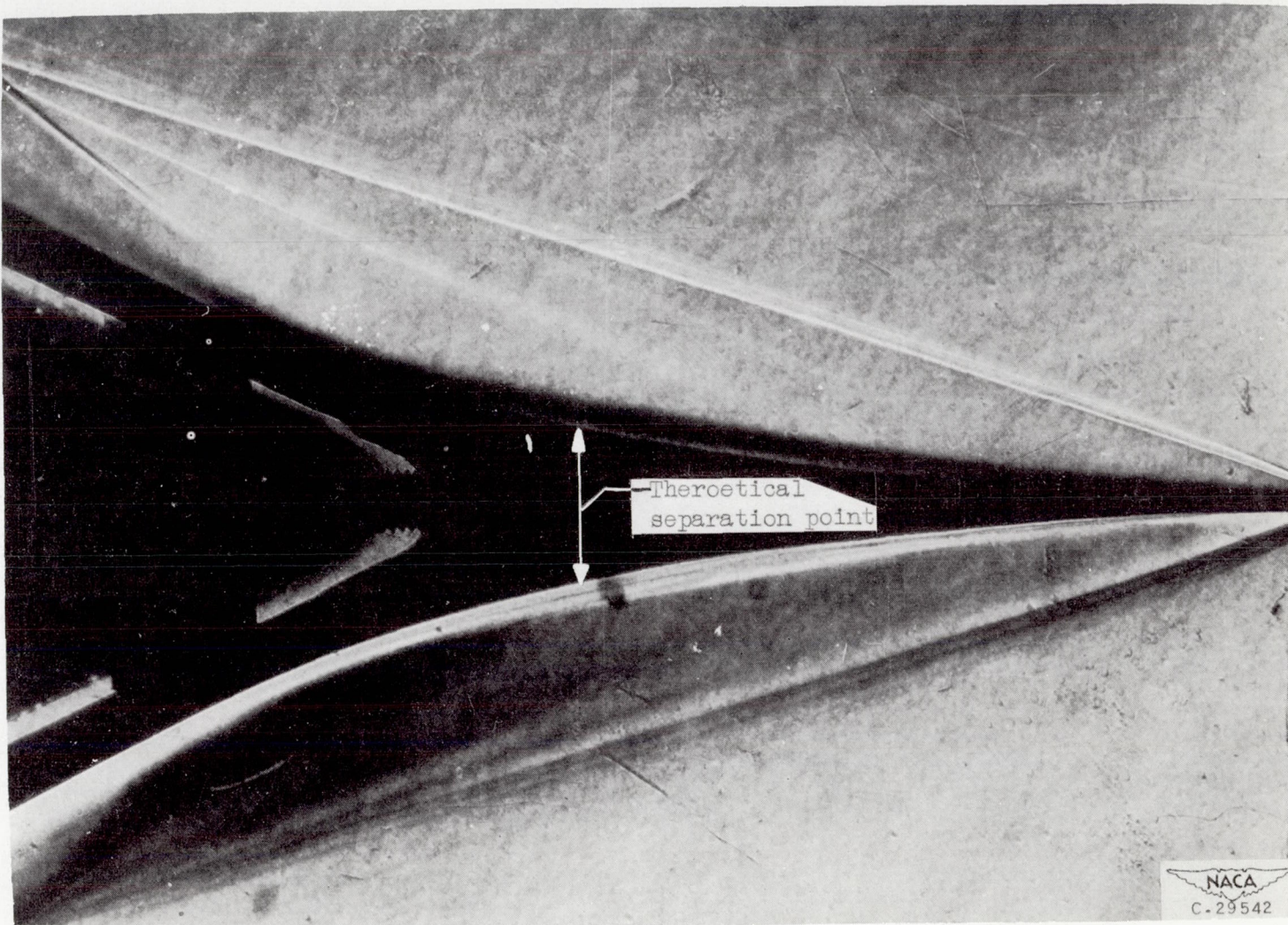
(d) Pressure instrumentation.

Figure 1. - Continued. Experimental model.



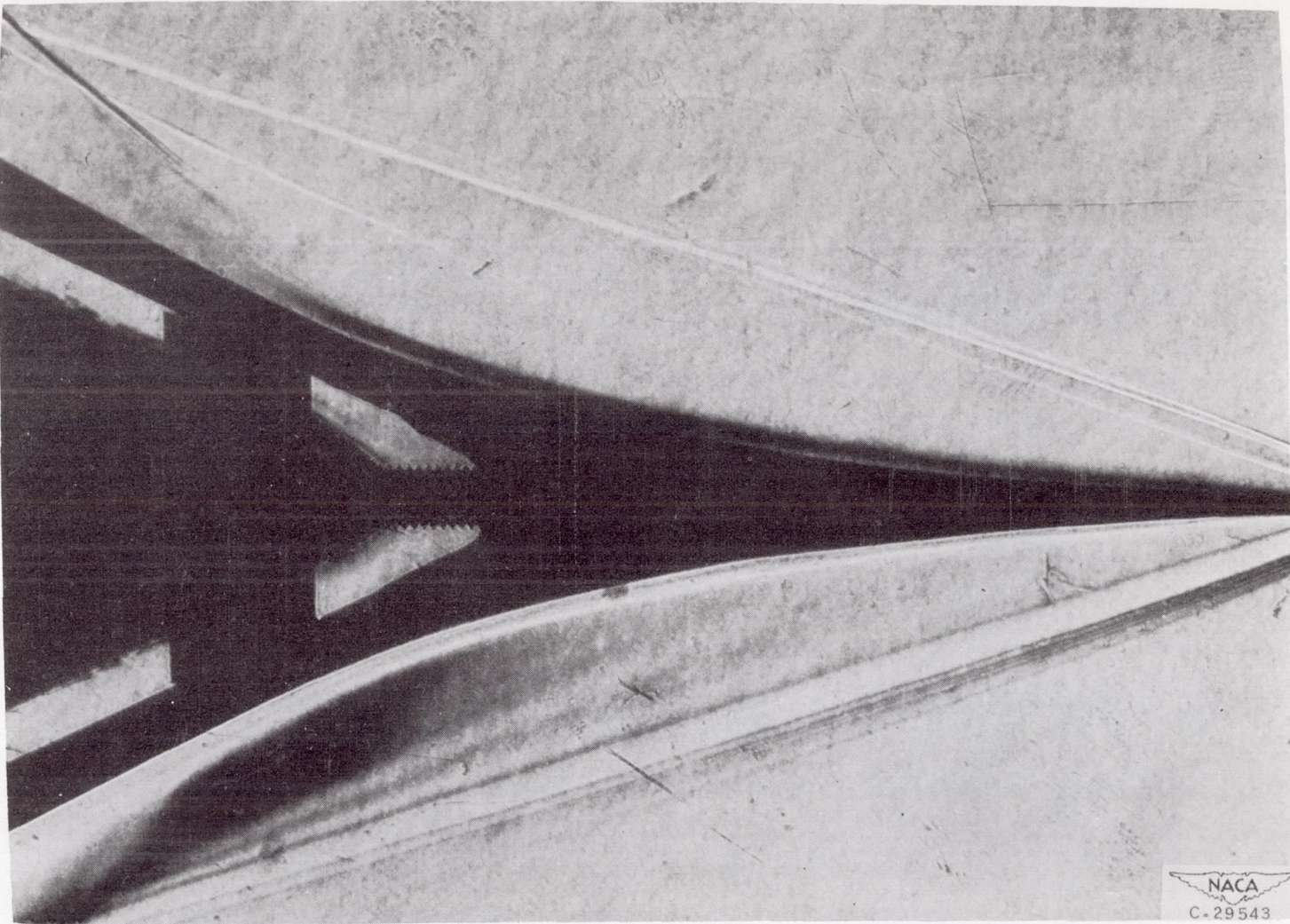
(e) Coordinate dimensions of original and modified inlets. Shaded sections indicate modifications to original design. Primed values of  $y$ ,  $z$ , and  $D$  are the coordinates of the modified inlet.

Figure 1. - Concluded. Experimental model.



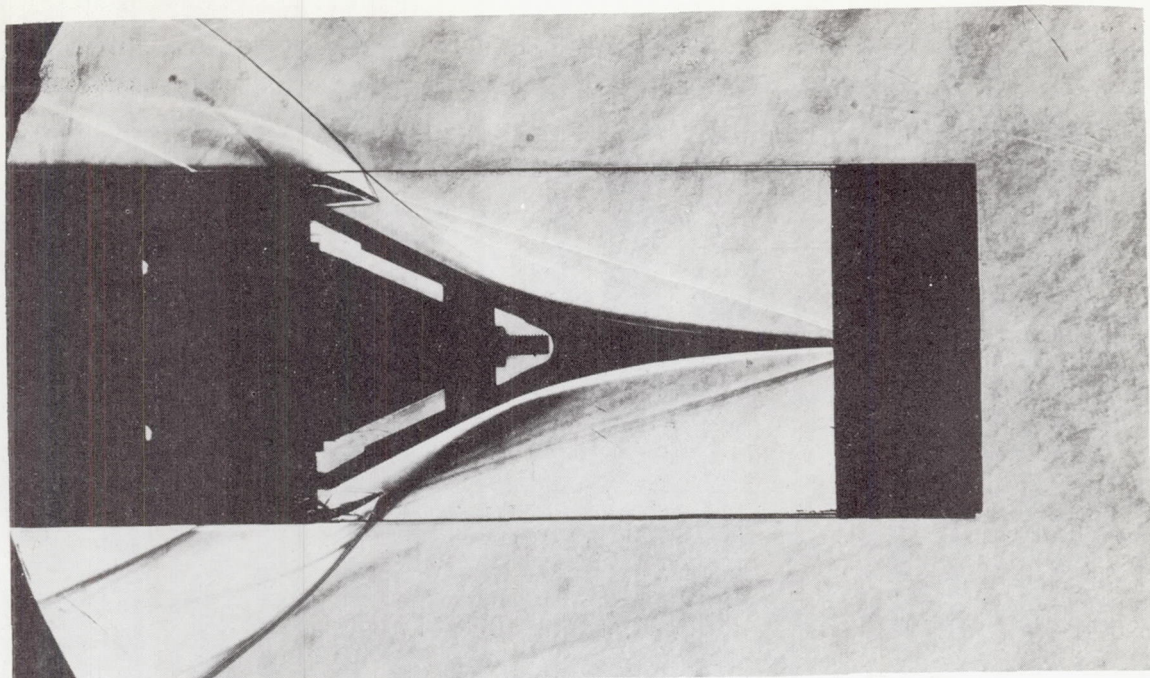
(a) With smooth leading edge.

Figure 2. - Schlieren photographs of flow along compression surfaces.

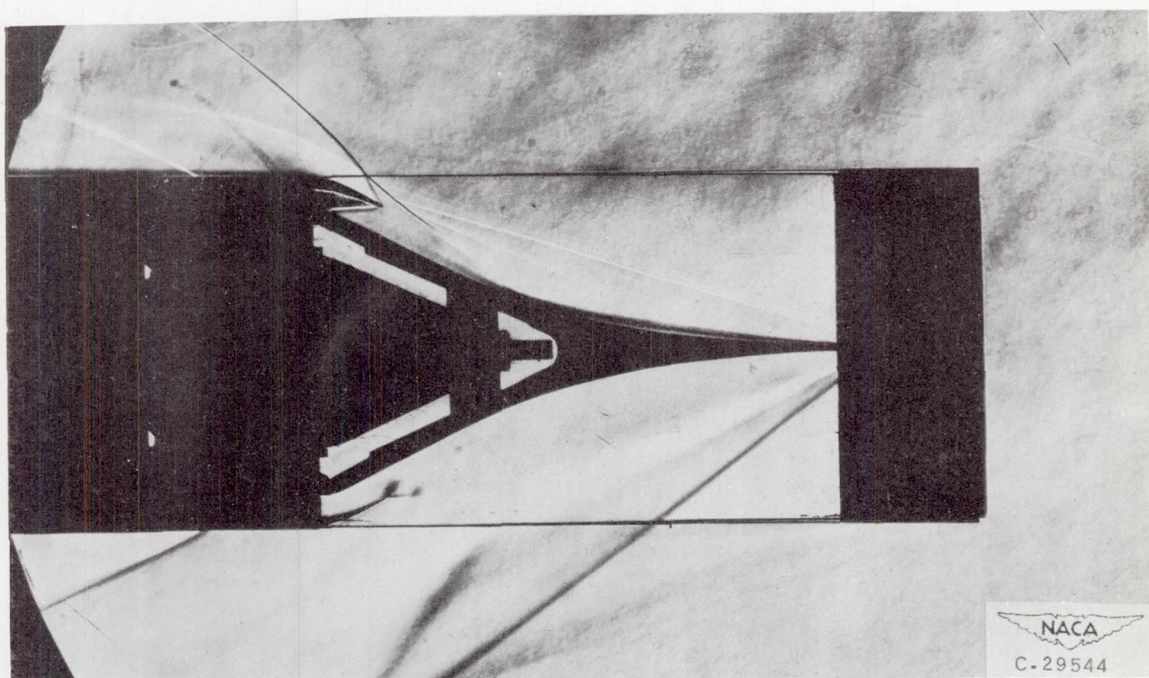


(b) With rough leading edge.

Figure 2. - Concluded. Schlieren photographs of flow along compression surfaces.



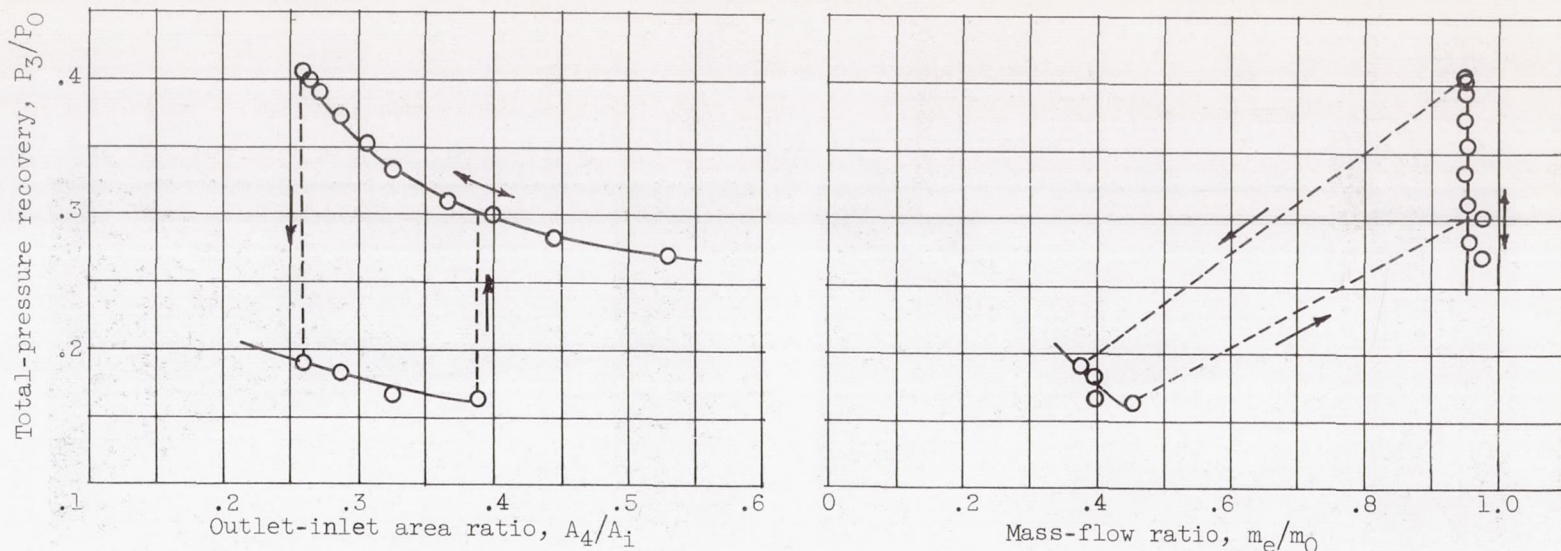
(a) Supercritical flow pattern.



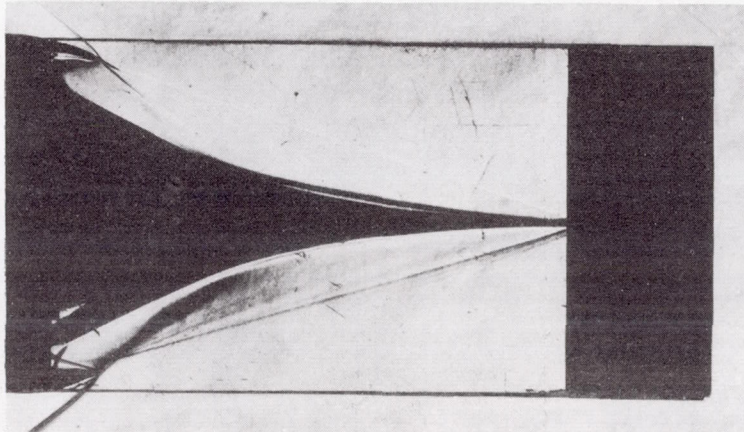
(b) Subcritical flow pattern.

Figure 3. - Schlieren photographs of shock configuration obtained with original inlet at optimum tip projection.

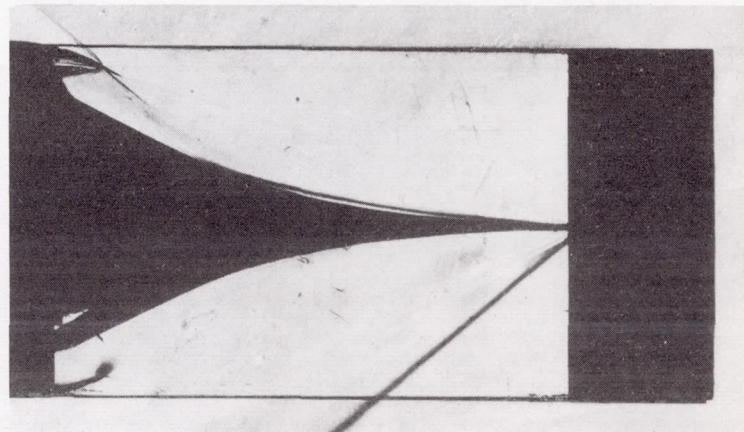
NACA  
C-29544



(a) Variation of total-pressure recovery with outlet-inlet area ratio and mass-flow ratio.



Supercritical flow pattern

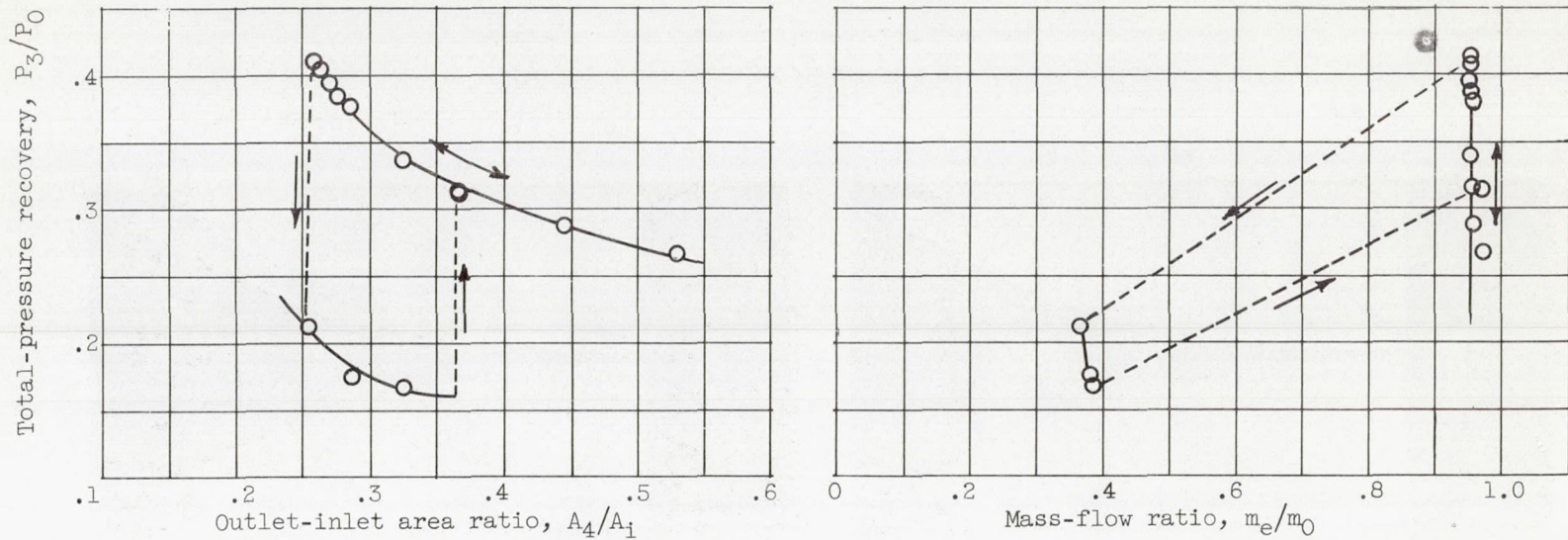


Subcritical flow pattern

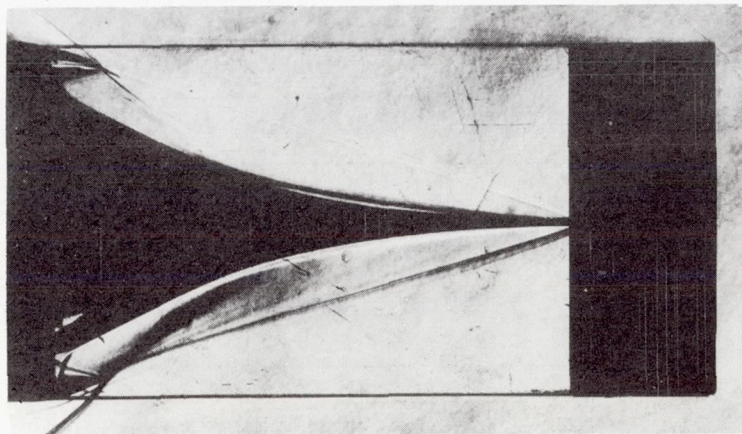
(b) Schlieren photographs of flow at diffuser inlet.

Figure 4. - Diffuser performance at zero angle of attack.

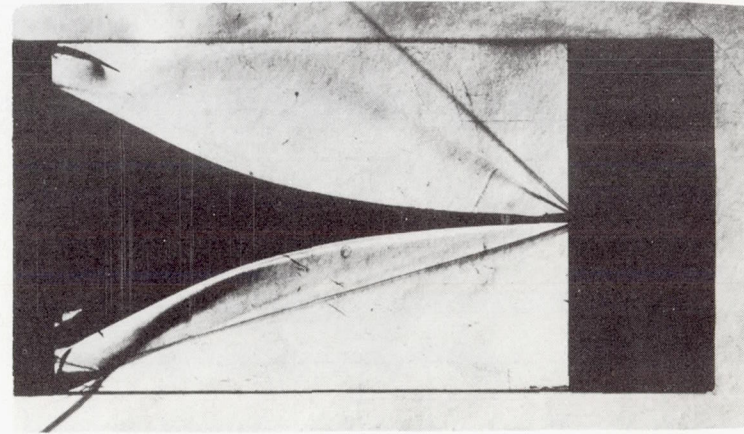
NACA  
C-29817



(a) Variation of total-pressure recovery with outlet-inlet area ratio and mass-flow ratio.



Supercritical flow pattern

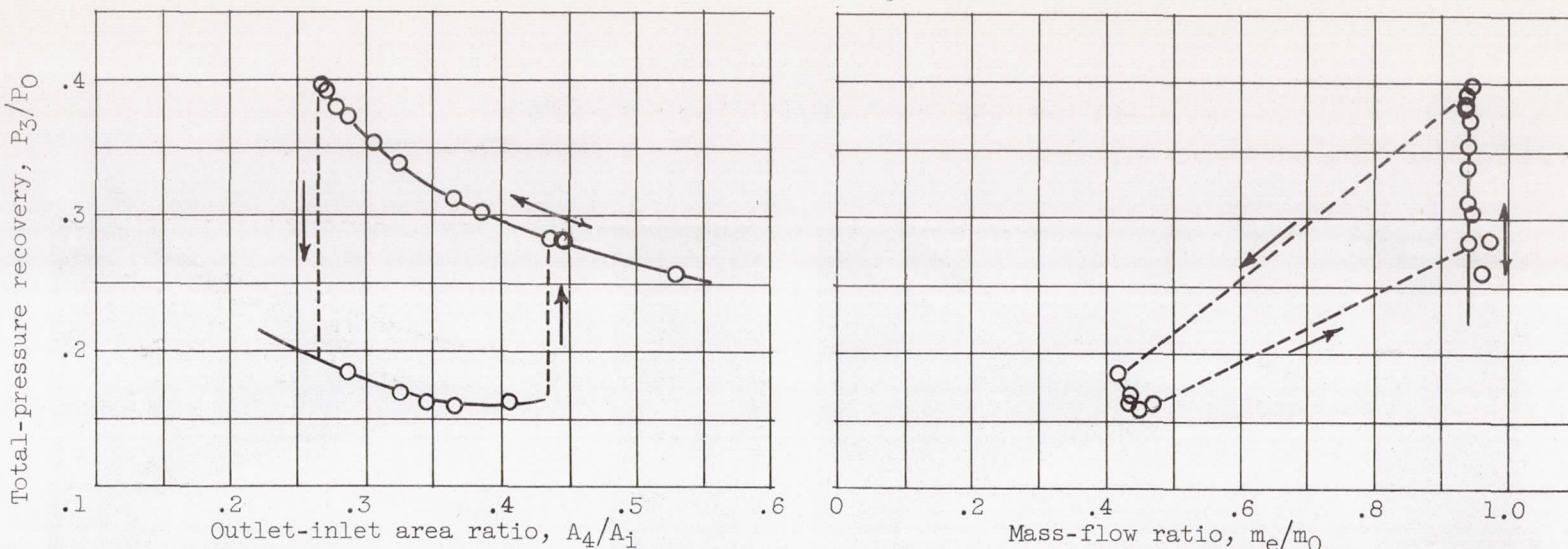


Subcritical flow pattern

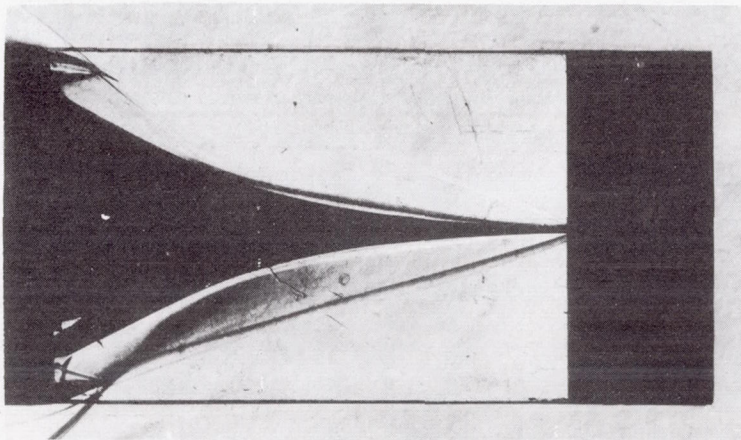
(b) Schlieren photographs of flow at diffuser inlet.

Figure 5. - Diffuser performance at  $1^\circ$  angle of attack.

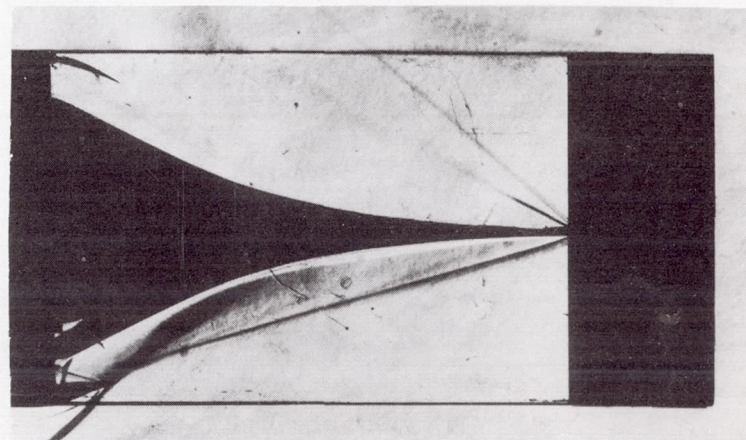
NACA  
C-29818



(a) Variation of total-pressure recovery with outlet-inlet area ratio and mass-flow ratio.



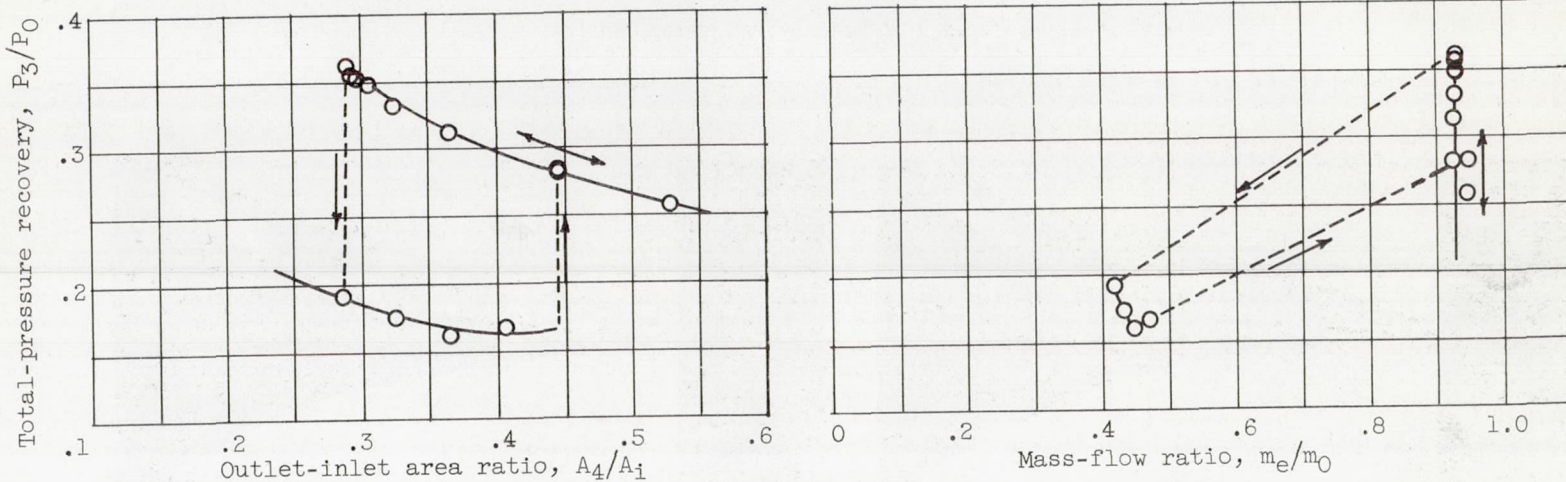
Supercritical flow pattern



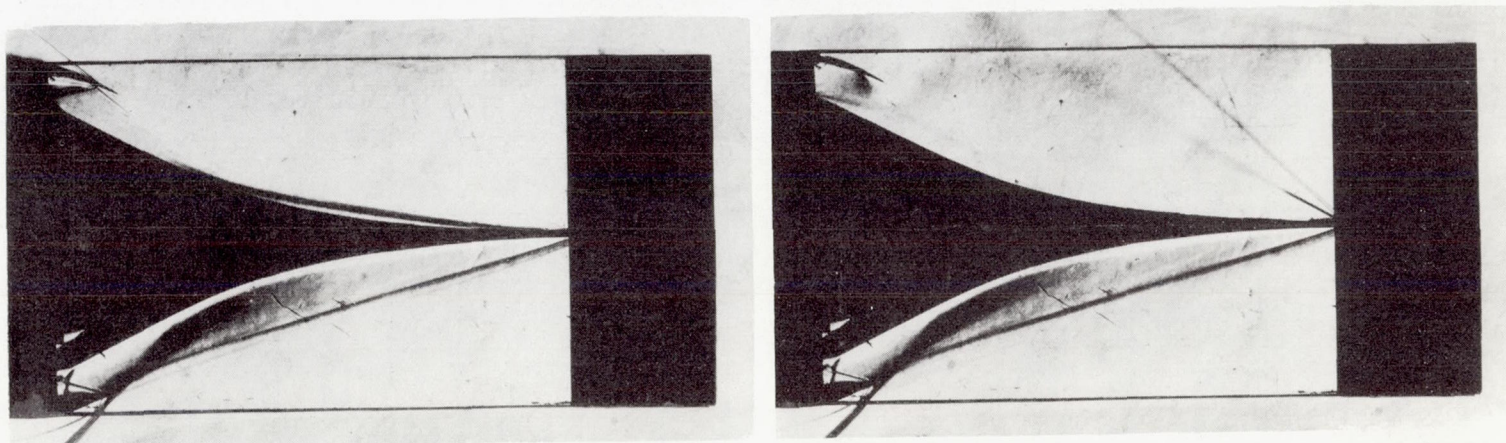
Subcritical flow pattern

(b) Schlieren photographs of flow at diffuser inlet.

Figure 6. - Diffuser performance at  $2^\circ$  angle of attack.



(a) Variation of total-pressure recovery with outlet-inlet area ratio and mass-flow ratio.



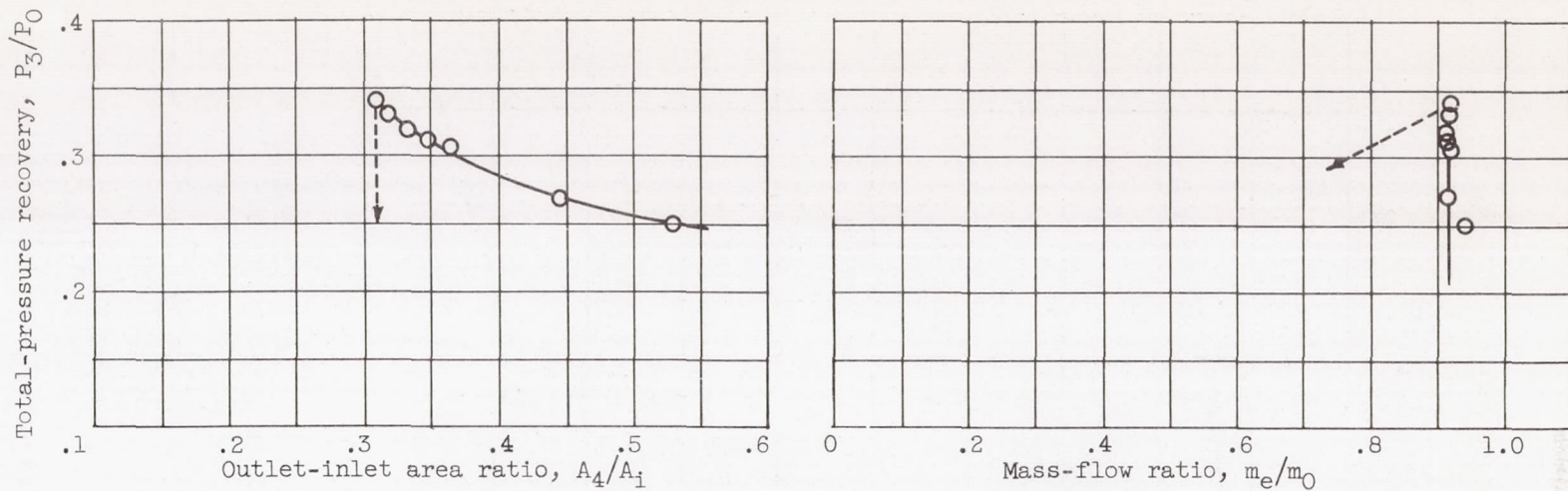
Supercritical flow pattern

Subcritical flow pattern

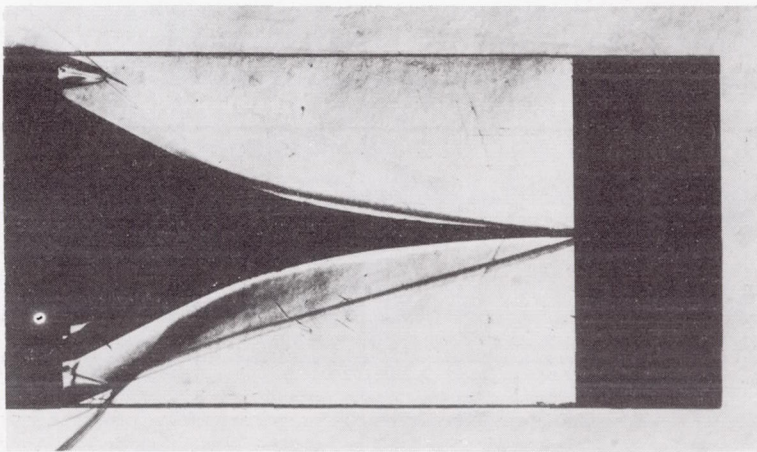
(b) Schlieren photographs of flow at diffuser inlet.

Figure 7. - Diffuser performance at  $3^\circ$  angle of attack.

NACA  
C-29820



(a) Variation of total-pressure recovery with outlet-inlet area ratio and mass-flow ratio.



NACA  
C-29821

(b) Schlieren photograph of supercritical flow pattern at diffuser inlet.

Figure 8. - Diffuser performance at  $4^\circ$  angle of attack.

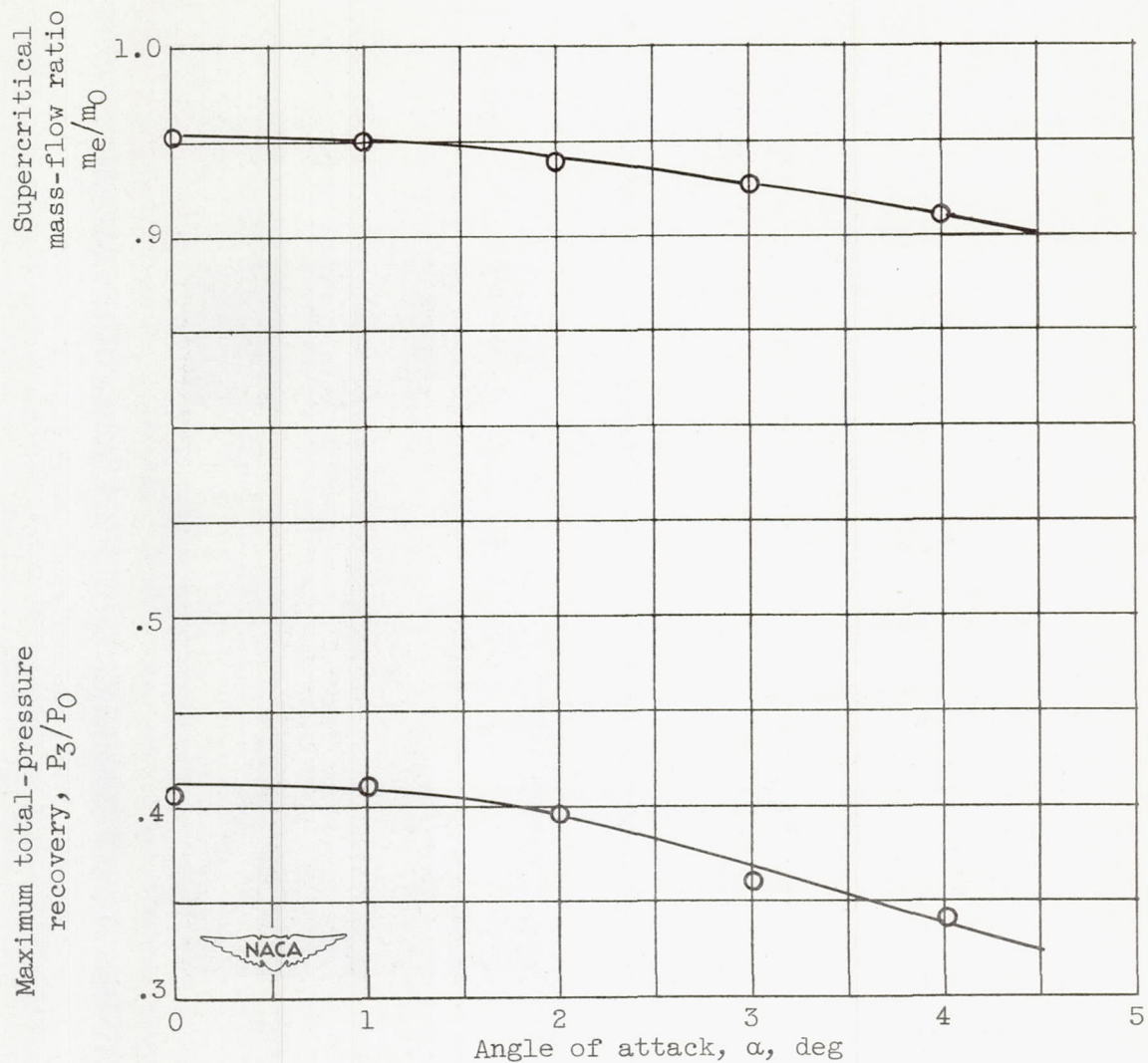


Figure 9. - Effect of angle of attack on maximum total-pressure recovery and supercritical mass-flow ratio.

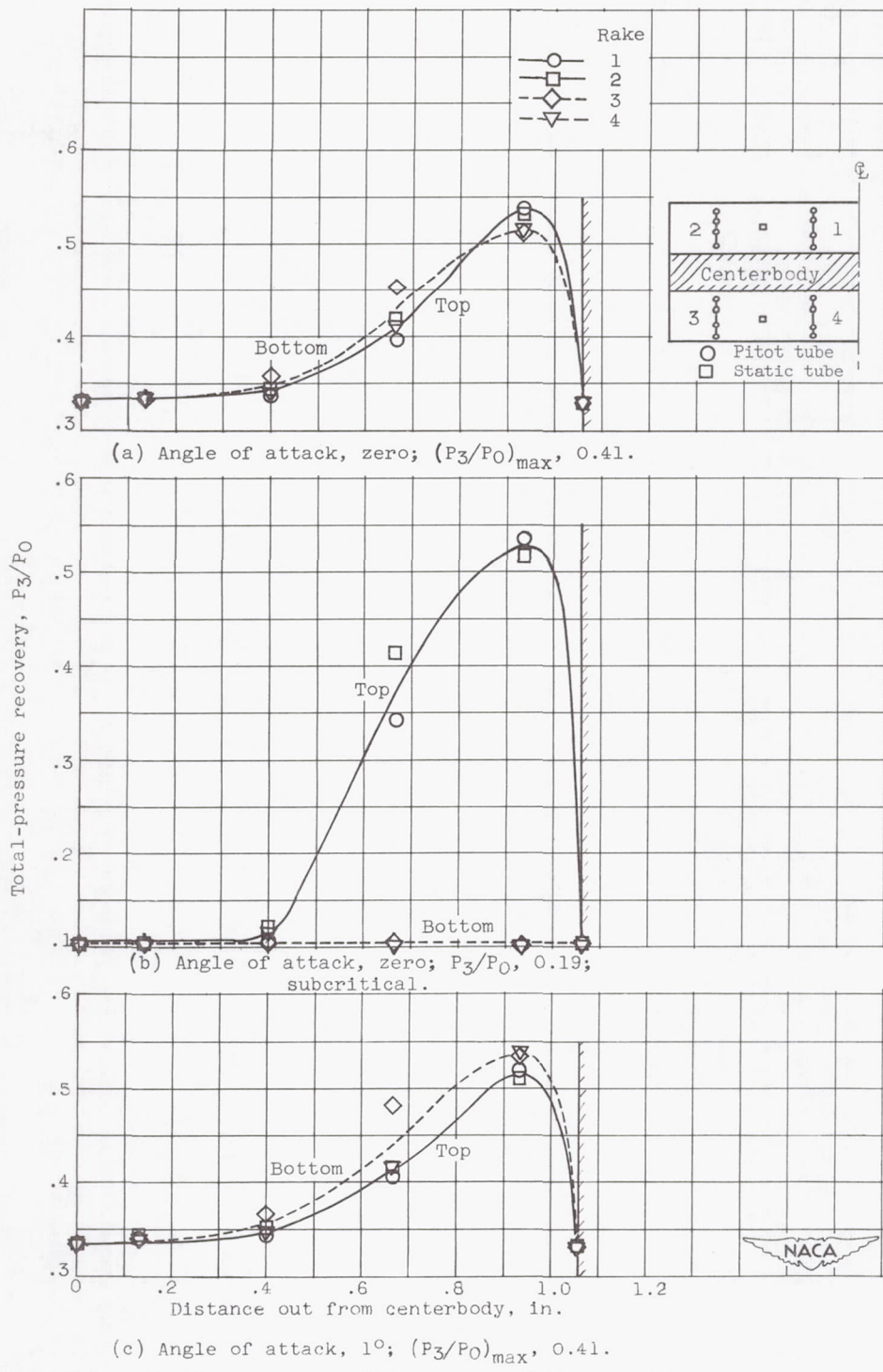


Figure 10. - Total-pressure profiles across diffuser exit.

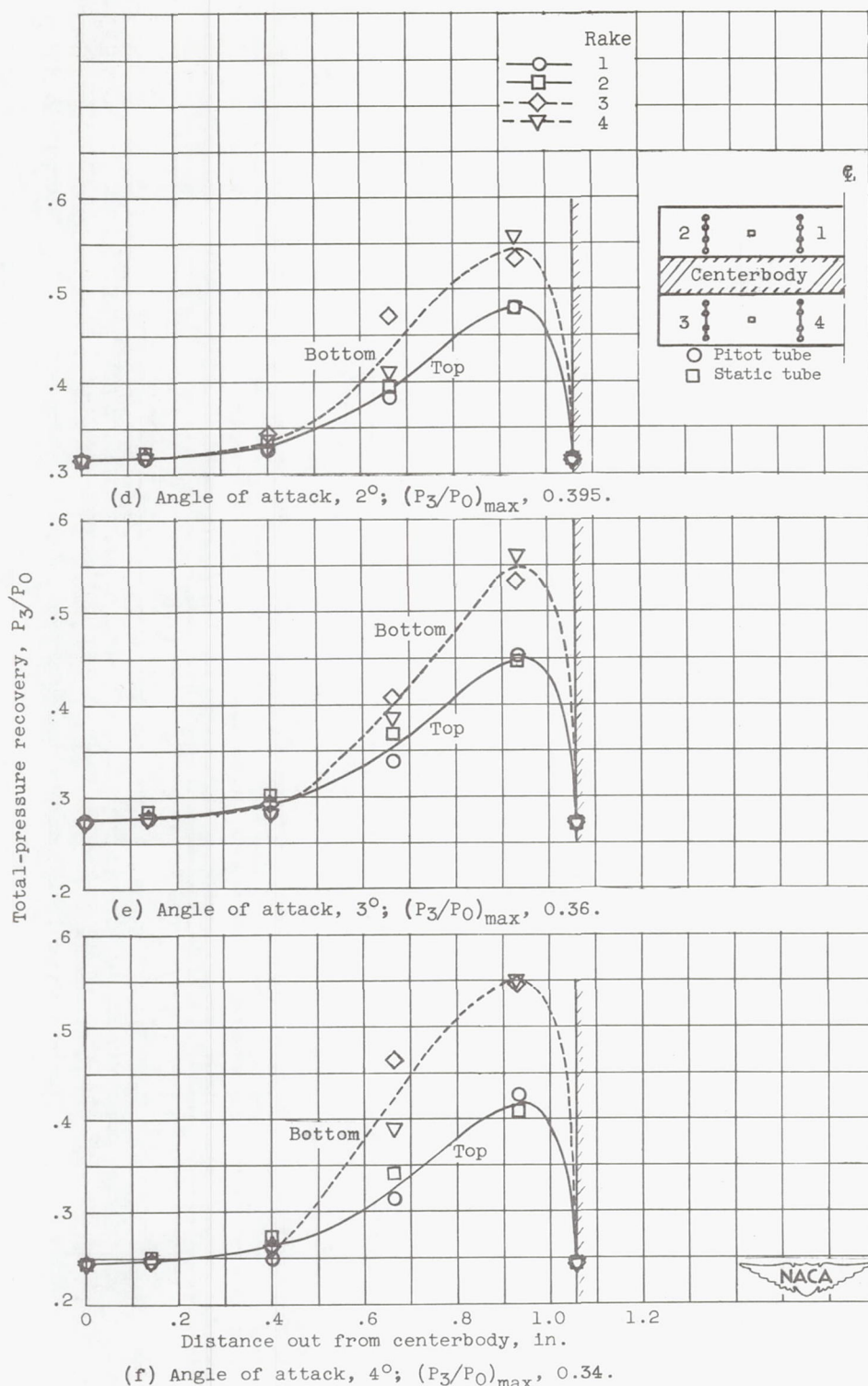


Figure 10. - Concluded. Total-pressure profiles across diffuser exit.

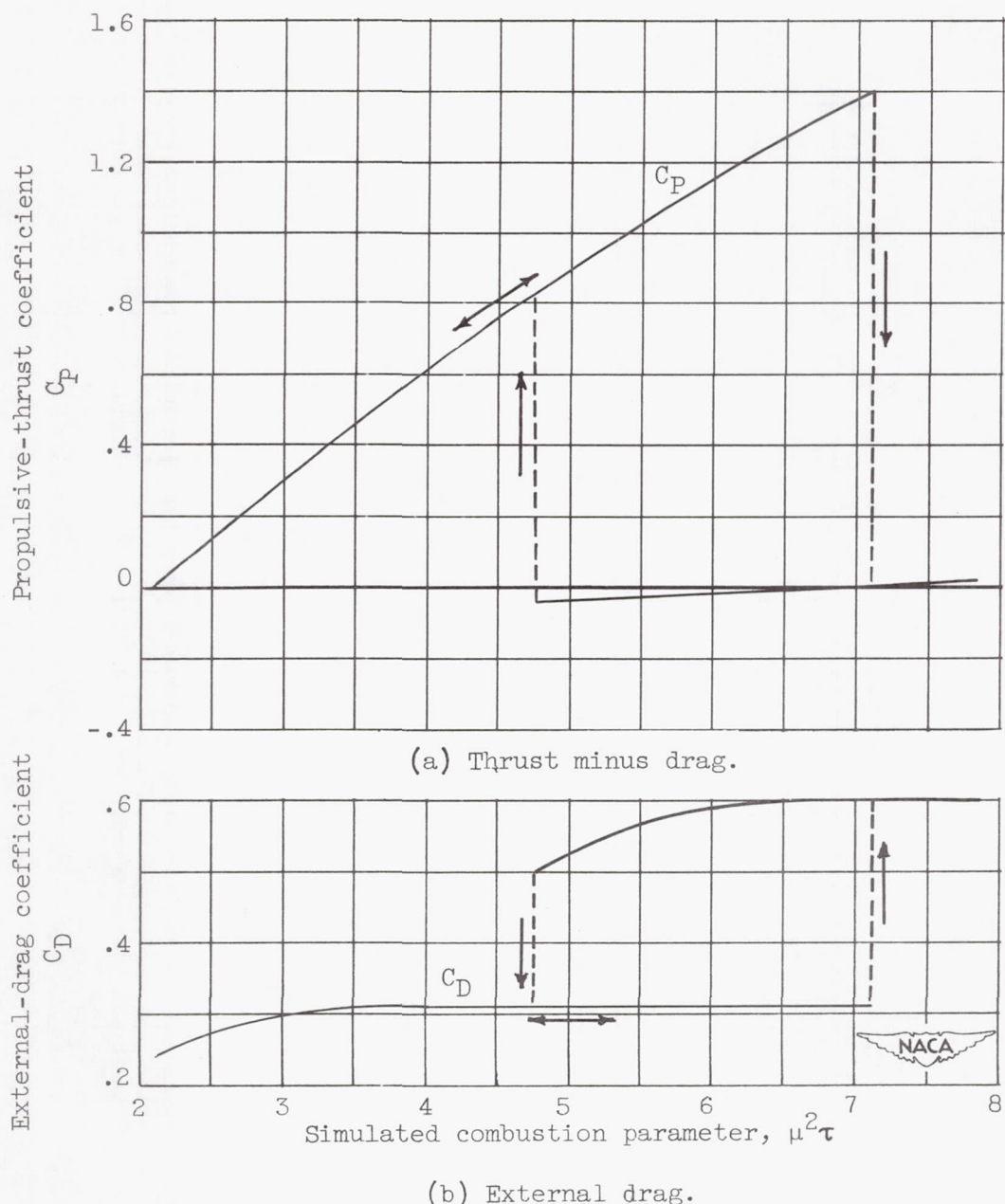


Figure 11. - Force coefficients as function of simulated combustion parameter  $\mu^2\tau$  at zero angle of attack.

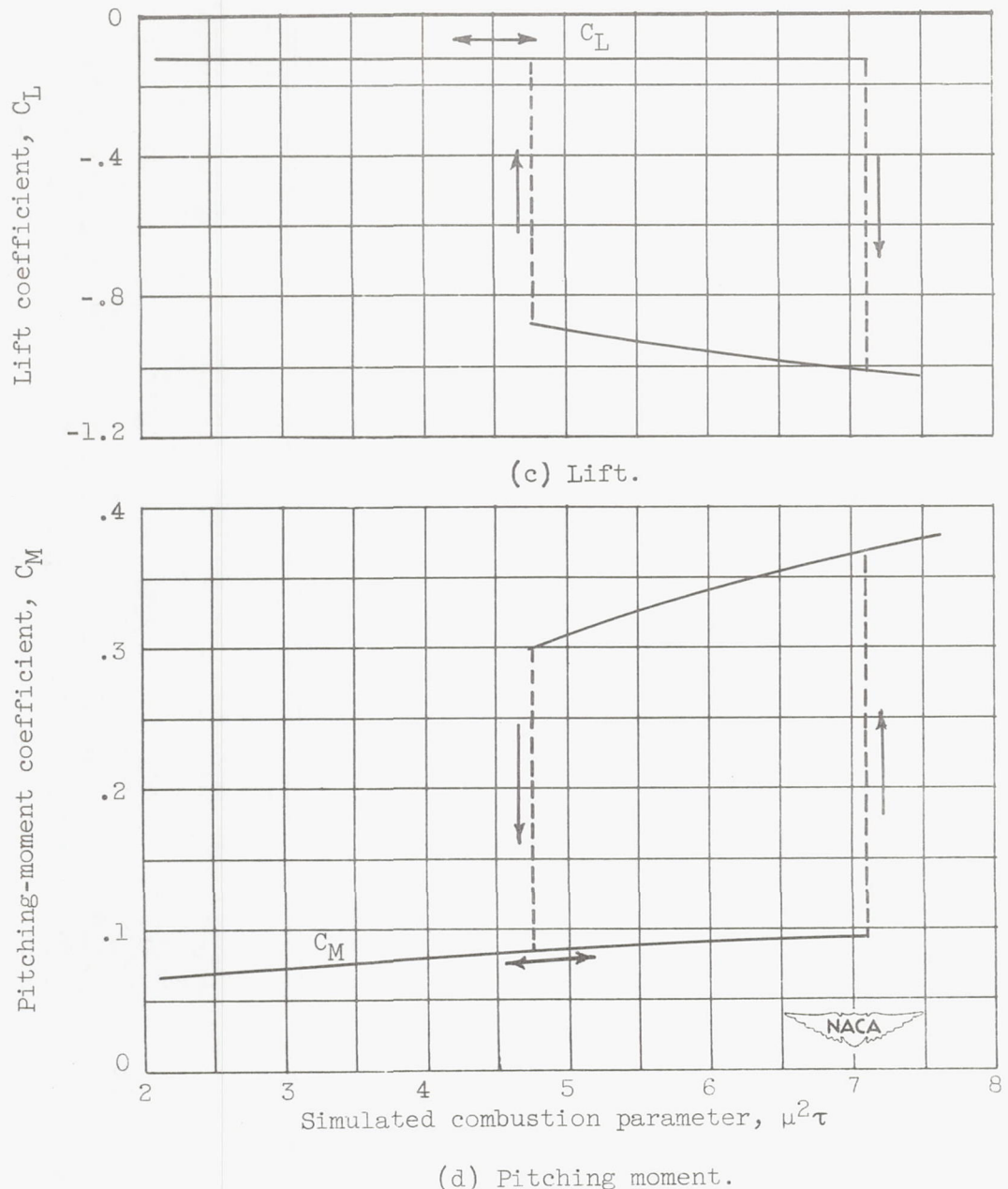


Figure 11. - Concluded. Force coefficients as function of simulated combustion parameter  $\mu^2\tau$  at zero angle of attack.